Supplementary Information

Building retrofits and urban climate feedback trigger heating energy rebounds and inequity

Yiqing Liu[1,2], Sue Grimmond[2]*, Zhiwen Luo[3]*

[1] School of Built Environment, University of Reading, Reading, United Kingdom

[2] Department of Meteorology, University of Reading, Reading, United Kingdom

[3] Welsh School of Architecture, Cardiff University, Cardiff, United Kingdom

*Correspondence: Prof Zhiwen Luo (luoz18@cardiff.ac.uk); Prof Sue Grimmond (c.s.grimmond@reading.ac.uk)

SI 1. $Q_{F,B}$ calculation and parametrisation

To calculate anthropogenic heat emission from building ($Q_{F,B}$), each component of Eq. (1) is derived from heat flux difference between an 'occupied' (*o*) and 'unoccupied' (*uo*) state[1]. The '*uo*' state represents a pre-occupation empty building, with the difference (Δ=*o*-*uo*) between the two states capturing heat fluxes resulting from human activities. This allows us to isolate the changed heat fluxes induced by human activities only.

Beyond the main formulation in Eq. (1), internal heat gains in the IECC (International Energy Conservation Code) archetypes are partitioned into radiant, sensible, latent, and lost fractions. The "lost" fraction does not impact the building's energy balance but accounts for within building energy use, indicating its heat emission should also be considered. As we assume all "lost" heat from most appliances (e.g. cooking ranges and miscellaneous equipment) is sensible heat exhausted via mechanical ventilation, its emissions are included in ΔBAE (building air exchange in Eq. (1)). For gas clothes-dryers releasing humid waste air to outdoors, we assume 60% being sensible for inclusion in $Q_{F,B}$[2]. For washing machines and dishwashers, the heat is transferred to hot water, leaving the building volume via pipe network and is currently unaccounted for in $Q_{F,B}$.

In each city, the EnergyPlus determined daily mean $Q_{F,B}$ is used to parameterise $Q_{F,B}$ based on heating/cooling degree days (HDD/CDD) allowing some weather variability to be accounted for [3,4]:

$$Q_{F,B} = \rho_{pop}[a_{F0} + a_{F1}CDD + a_{F2}HDD] \quad \text{(S1)}$$

$$CDD = \left|T_a - T_{b,c}\right| \; when \; T_a > T_{b,c} \quad \text{(S2)}$$

$$HDD = \left|T_{b,h} - T_a\right| \; when \; T_a < T_{b,h} \quad \text{(S3)}$$

where ρ_{pop} is the population density and T_a is daily mean outdoor air temperature. a_{F0}, a_{F1}, a_{F2}, are coefficients reflecting the base value of $Q_{F,B}$ and its sensitivity to CDD and HDD. Here, these coefficients and base temperatures for heating ($T_{b,h}$) and cooling ($T_{b,c}$) are determined from the EnergyPlus daily mean $Q_{F,B}$ and urbanised the 2-m outdoor air temperature (T_a) from TMY3.

The diurnal variations of $Q_{F,B}$ affect outdoor energy exchanges, with timing important because of the growth and decay of the boundary layer[5,6,7] when large $Q_{F,B}$ can be influenced by building operations (profiles corresponding to heating, cooling or ventilation)[8]. We give SUEWS three median diurnal profiles (hourly $Q_{F,B}$ is normalised by daily mean $Q_{F,B}$) that vary with outdoor air temperature (heating ($T_a < T_{b,h}$), cooling ($T_a > T_{b,c}$) and ventilation ($T_{b,c} > T_a > T_{b,h}$) in Table S1-S2) to more accurately reflect the temporal dynamics of $Q_{F,B}$.

Table S1 Neighbourhood scale $Q_{F,B}$ coefficients for Eq. S1- S3 determined from EnergyPlus daily mean results for before retrofitting (BR) scenarios, assuming all buildings are base case (BC) building.

Climate zone	$T_{b,h}$ [°C]	$T_{b,c}$ [°C]	a_{F0} [W m^{-2} (Cap ha^{-1})$^{-1}$]	a_{F1} [W m^{-2} K^{-1}(Cap ha^{-1})$^{-1}$]	a_{F2} [W m^{-2} K^{-1}(Cap ha^{-1})$^{-1}$]
1A	22.0	24.0	0.0776	0.0065	0.0090
2A	21.1	24.0	0.0839	0.0044	0.0117
2B	21.6	24.0	0.1054	0.0038	0.0092
3A	17.5	24.0	0.1022	0.0025	0.0215
3B	19.3	24.0	0.1032	0.0043	0.0136
3C	18.5	21.3	0.1022	0.0082	0.0124
4A	15.8	24.0	0.1004	0.0041	0.0297
4B	16.5	24.0	0.1130	0.0034	0.0177
4C	14.9	16.0	0.1355	0.0000	0.0256
5A	15.2	24.0	0.1181	0.0000	0.0312
5B	16.5	22.5	0.1206	0.0058	0.0206
5C	12.6	16.0	0.1510	0.0012	0.0255
6A	14.2	21.8	0.0983	0.0046	0.0243
6B	15.3	24.0	0.1395	0.0031	0.0247
7	12.0	22.0	0.0960	0.0061	0.0216
8	12.0	12.0	0.0769	0.0036	0.0225

Table S2 As Table S2, but for after retrofitting (AR) scenario varied by 4 retrofit adoption rate ($n_{retrofit}$=25%, 50%, 75% and 95%).

Climate zone	$T_{b,h}$ [°C]	$T_{b,c}$ [°C]	a_{F0} [W m^{-2} (Cap ha^{-1})$^{-1}$]	a_{F1} [W m^{-2} K^{-1}(Cap ha^{-1})$^{-1}$]	a_{F2} [W m^{-2} K^{-1}(Cap ha^{-1})$^{-1}$]
$n_{retrofit}$=25%					
1A	21.9	24.0	0.0706	0.0062	0.0071
2A	19.5	24.0	0.0808	0.0032	0.0107
2B	21.4	24.0	0.0940	0.0038	0.0075
3A	17.1	24.0	0.0909	0.0031	0.0175
3B	18.6	24.0	0.0931	0.0041	0.0111
3C	18.3	21.0	0.0898	0.0068	0.0098
4A	15.5	24.0	0.0896	0.0048	0.0239
4B	16.0	24.0	0.1004	0.0041	0.0143
4C	14.8	14.2	0.1154	0.0003	0.0208
5A	15.0	24.0	0.1032	0.0002	0.0253
5B	16.0	22.5	0.1075	0.0052	0.0167
5C	12.5	16.0	0.1274	0.0021	0.0209
6A	14.1	21.3	0.0880	0.0044	0.0202
6B	15.1	24.0	0.1212	0.0049	0.0200
7	12.0	21.6	0.0859	0.0060	0.0179
8	12.0	12.0	0.0686	0.0036	0.0187
$n_{retrofit}$=50%					
1A	20.8	24.0	0.0644	0.0056	0.0061
2A	18.9	24.0	0.0724	0.0034	0.0088
2B	20.8	24.0	0.0829	0.0038	0.0060

3A	16.7	24.0	0.0786	0.0040	0.0135
3B	17.8	24.0	0.0816	0.0041	0.0085
3C	17.6	21.0	0.0782	0.0059	0.0074
4A	15.1	24.0	0.0789	0.0054	0.0182
4B	14.9	24.0	0.0880	0.0048	0.0110
4C	14.6	15.7	0.0941	0.0015	0.0161
5A	14.7	23.8	0.0888	0.0019	0.0194
5B	15.6	22.4	0.0918	0.0052	0.0127
5C	12.4	16.0	0.1036	0.0031	0.0162
6A	14.0	20.9	0.0777	0.0046	0.0161
6B	14.7	23.9	0.1025	0.0065	0.0154
7	12.0	21.6	0.0754	0.0067	0.0141
8	12.0	12.0	0.0603	0.0036	0.0149
$n_{retrofit}$=75%					
1A	20.8	24.0	0.0644	0.0056	0.0061
2A	18.9	24.0	0.0724	0.0034	0.0088
2B	20.8	24.0	0.0829	0.0038	0.0060
3A	16.7	24.0	0.0786	0.0040	0.0135
3B	17.8	24.0	0.0816	0.0041	0.0085
3C	17.6	21.0	0.0782	0.0059	0.0074
4A	15.1	24.0	0.0789	0.0054	0.0182
4B	14.9	24.0	0.0880	0.0048	0.0110
4C	14.6	15.7	0.0941	0.0015	0.0161
5A	14.7	23.8	0.0888	0.0019	0.0194
5B	15.6	22.4	0.0918	0.0052	0.0127
5C	12.4	16.0	0.1036	0.0031	0.0162
6A	14.0	20.9	0.0777	0.0046	0.0161
6B	14.7	23.9	0.1025	0.0065	0.0154
7	12.0	21.6	0.0754	0.0067	0.0141
8	12.0	12.0	0.0603	0.0036	0.0149
$n_{retrofit}$=95%					
1A	18.8	24.0	0.0507	0.0052	0.0030
2A	17.4	24.0	0.0546	0.0045	0.0048
2B	18.3	24.0	0.0617	0.0039	0.0032
3A	14.3	22.3	0.0540	0.0041	0.0063
3B	14.9	21.6	0.0547	0.0036	0.0037
3C	14.2	19.9	0.0525	0.0041	0.0037
4A	13.0	20.9	0.0538	0.0041	0.0078
4B	12.0	18.6	0.0556	0.0032	0.0047
4C	14.0	15.2	0.0534	0.0033	0.0074
5A	13.0	21.1	0.0595	0.0036	0.0087
5B	12.8	21.6	0.0628	0.0044	0.0054
5C	12.0	14.4	0.0578	0.0034	0.0077
6A	13.0	19.7	0.0588	0.0041	0.0085
6B	13.6	17.2	0.0623	0.0029	0.0069
7	12.0	15.5	0.0526	0.0027	0.0073
8	12.0	12.0	0.0450	0.0037	0.0079

Table S3 Thermal properties used from dominant probability for single family detached house constructed before 1980 in RESSTOCK (Wilson et al., 2017; Reyna et al., 2022).

City	R_wall ($°F \cdot ft^2 \cdot h\ BTU^{-1}$)	R_ceiling ($°F \cdot ft^2 \cdot h\ BTU^{-1}$)	Window type	Window U-value ($W\ m^{-2} K^{-1}$)	SHGC	Infiltration (ACH at 50Pa)
1A Miami, FL	0	13	Single, Clear, Metal	6.59	0.76	20
2A Tampa, FL	0	13	Single, Clear, Non-metal	4.77	0.63	20
2B Tucson, AZ	0	13	Single, Clear, Non-metal	4.77	0.63	15
3A Atlanta, GA	0	13	Single, Clear, Non-metal	4.77	0.63	15
3B El Paso, TX	0	13	Single, Clear, Non-metal	4.77	0.63	15
3C San Diego, CA	0	13	Single, Clear, Non-metal	4.77	0.63	15
4A New York, NY	0	19	Single, Clear, Non-metal	4.77	0.63	15
4B Albuquerque, NM	0	13	Single, Clear, Non-metal	4.77	0.63	15
4C Seattle, WA	0	19	Single, Clear, Non-metal	4.77	0.63	15
5A Buffalo, NY	0	19	Single, Clear, Non-metal	4.77	0.63	15
5B Denver, CO	0	19	Single, Clear, Non-metal	4.77	0.63	15
5C Port Angeles, WA	0	19	Single, Clear, Non-metal	4.77	0.63	15
6A Rochester, MN	11	49	Single, Clear, Non-metal	4.77	0.63	15
6B Great Falls, MT	0	19	Double, Clear, Non-metal, Air	2.78	0.56	15
7 International Falls, MN	11	49	Double, Clear, Non-metal, Air	2.78	0.56	15
8 Fairbanks, AK	11	49	Double, Clear, Non-metal, Air	2.78	0.56	15

SI 2. ΔQ_S calculation and parametrisation

The net change in stored energy within the building volume (ΔQ_S) is calculated as the sum of two EnergyPlus outputs: *Surface Heat Storage Rate* and *Zone Air Heat Balance Air Energy Storage Rate*. The EnergyPlus-derived ΔQ_S, together with $Q_{F,B}$, are used to determine neighbourhood scale parameters prior to neighbourhood simulations.

Neighbourhood-scale storage heat flux is estimated using the Objective Hysteresis Model (OHM) [11]

$$\Delta Q_s = \sum_i f_i \left[a_{1i} Q^* + a_{2i} \frac{\partial Q^*}{\partial t} + a_{3i} \right] \quad \text{(S4)}$$

where f is the surface cover fraction for each surface type (seven per model grid-cell: paved, buildings, evergreen trees/shrubs, deciduous trees/shrubs, grass, bare soil and water), and three OHM coefficients (a_1, a_2, and a_3) determined from model simulations[12,13] or from observations[14,15]. These coefficients indicate the general proportional of Q^* that goes into ΔQ_S (a_1), degree of diurnal hysteresis between ΔQ_S and Q^* (a_2) and the size of the flux when Q^* is 0 W m^{-2} (a_3). The OHM coefficients are determined also from the initial EnergyPlus simulations. As the daily coefficients are highly influenced by wind speed at building height (U_{zh}) and incoming shortwave radiation ($K_\downarrow$), we parameterise a_1, a_2, a_3 as linear functions of U_{zh} and $K_\downarrow$ to capture the weather variability.

SI 3. SUEWS simulation iteration

Surface Urban Energy and Water Balance Scheme (SUEWS) is a neighbourhood or local-scale land surface model for simulating the surface energy fluxes[16] and vertical meteorological profiles[17,18,19], such as air temperature, wind speed, and relative humidity, within the roughness. The model has been extensively evaluated in many urban environments globally[16,17,18,19,20]. SUEWS allows rapid computation of the impacts of varying urban characteristics, such as land cover [21], neighbourhood

morphology[22], population increases[23] and building HVAC systems [24]. Therefore, we select this model to assess neighbourhood climate and impacts of building energy retrofitting.

The neighbourhood scale surface energy balance is written as[25]:

$$Q^* + Q_F = Q_H + Q_E + \Delta Q_S \quad \text{(S5)}$$

where Q^* is the net all-wave radiation, Q_F is the total anthropogenic heat flux, Q_H is the turbulent sensible heat flux, Q_E is the latent heat flux and ΔQ_S is the net storage heat flux. As SUEWS calculates Q_H as the residual in Eq. S5, the net changes from the other fluxes impact Q_H, consistent with observations[26].

The air temperature (T), humidity (q) and wind speed (U) at different heights (z) within urban canopy layer are expressed as [18, 19]:

$$T(z) = T(z_h) - \frac{Q_H}{u^* \rho c_p} \frac{P_r}{\beta f}\left[1 - e^{\left(\frac{\beta f (z - z_h)}{l_M}\right)}\right] \quad \text{(S6)}$$

$$q(z) = q(z_h) - \frac{Q_E}{u^* \rho L_v} \frac{P_r}{\beta f}\left[1 - e^{\left(\frac{\beta f (z - z_h)}{l_M}\right)}\right] \quad \text{(S7)}$$

$$U(z) = U(z_h)\, e^{\left(\frac{\beta (z - z_h)}{l_M}\right)} \quad \text{(S8)}$$

where z_h is urban canopy layer height assumed here to be mean building height, u^* friction velocity, ρ density of air, c_p the specific heat of air at constant pressure, P_r the Prandtl number, and l_M the mixing length. β and f are the Harman and Finnigan (2007) parameters, L_v the latent heat of vaporisation.

After determining the coefficients for both $Q_{F,B}$ and ΔQ_S (Section SI.1 and SI.2), SUEWS is run iteratively until 2 m air temperature converges (<0.01 °C; Fig. S1). An initial $Q_{F,B}$ is obtained by calculating HDD and CDD from initial forcing air temperature $T_{forcing}$ in SUEWS, producing an updated air temperature T_2. This T_2 is used to calculate the new $Q_{F,B}$. Initial OHM coefficients (derived from statistical regression for one-year hourly ΔQ_S and Q^*, SI 2) are used to calculate ΔQ_S, with wind speed at building height (U_{zh}) used to update OHM coefficients and ΔQ_S iteratively. Convergence is typically achieved within three iterations.

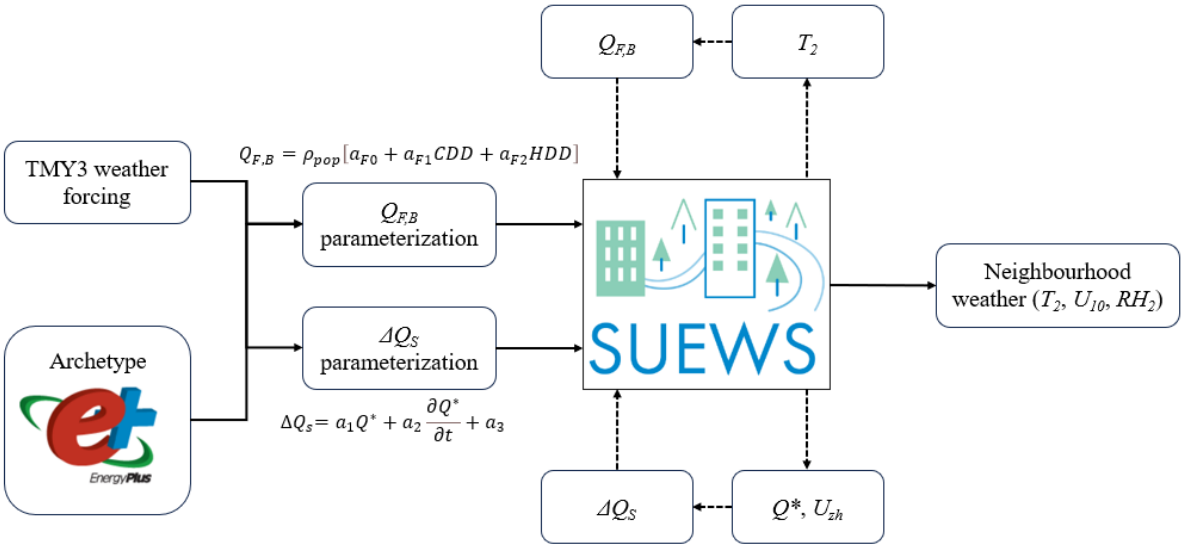

Fig. S1: Workflow of determining SUEWS model parameters for ΔQ_S and $Q_{F,B}$ and simulations. Internal SUEWS iteration processes (dashed) update ΔQ_S and $Q_{F,B}$.

Table S4 Longitude and latitude for the ERA5 grid used as climate forcing in SUEWS.

City	Longitude (W °)	Latitude (N°)
1A Miami, FL	80.25	25.875
2A Tampa, FL	82.5	27.875
2B Tucson, AZ	111.0	32.25
3A Atlanta, GA	84.375	33.75
3B El Paso, TX	106.375	31.75
3C San Diego, CA	117.125	32.75
4A New York, NY	73.75	40.625
4B Albuquerque, NM	106.75	35.0
4C Seattle, WA	122.75	47.625
5A Buffalo, NY	78.875	42.875
5B Denver, CO	105.0	39.75
5C Port Angeles, WA	123.375	48.125
6A Rochester, MN	92.5	44.0
6B Great Falls, MT	111.375	47.5
7 International Falls, MN	93.375	48.625
8 Fairbanks, AK	147.475	64.75

SI 4. Change of heat flux from energy retrofit

Building energy retrofitting changes the wintertime neighbourhood anthropogenic ($Q_{F,B}$), storage (ΔQ_S) and turbulent sensible heat fluxes (Q_H) in different ways (Fig. 3). For the medium density scenario with 95% retrofit adoption rate, all cities has larger change in $Q_{F,B}$ than ΔQ_S. Their net effect impacts Q_H and therefore outdoor air temperature. The change in $Q_{F,B}$ has a clear diurnal pattern in most cities, with nocturnal reduction being more pronounced, most notably in colder regions such as Great Falls, International Falls and Fairbanks. Whereas, warmer cities with little need for heating (e.g. Miami and Tampa) have a negligible reduction in $Q_{F,B}$. This negative correlation between daily reduced $Q_{F,B}$ and $T_{forcing}$ holds generally (Fig. 4) as cities in the colder regions have higher initial heating demands, and those in warmer areas have smaller changes.

The relatively small change in ΔQ_S (Fig. S2) is attributed to the very lightweight envelope used in IECC archetype (wood-frame wall). Such lightweight material has limited capacity for heat absorption and release, constraining the magnitude of ΔQ_S. The energy retrofitting measures, such as enhanced insulation and lower windows solar heat gain coefficient (SHGC), further reduce daytime solar radiation driven gains (negative change from 09:00 to 15:00, Fig. S2), and therefore reducing heat release at night. It indicates for lightweight buildings, retrofitting primarily influences urban climate through changes in $Q_{F,B}$, rather than through modifications in building heat storage.

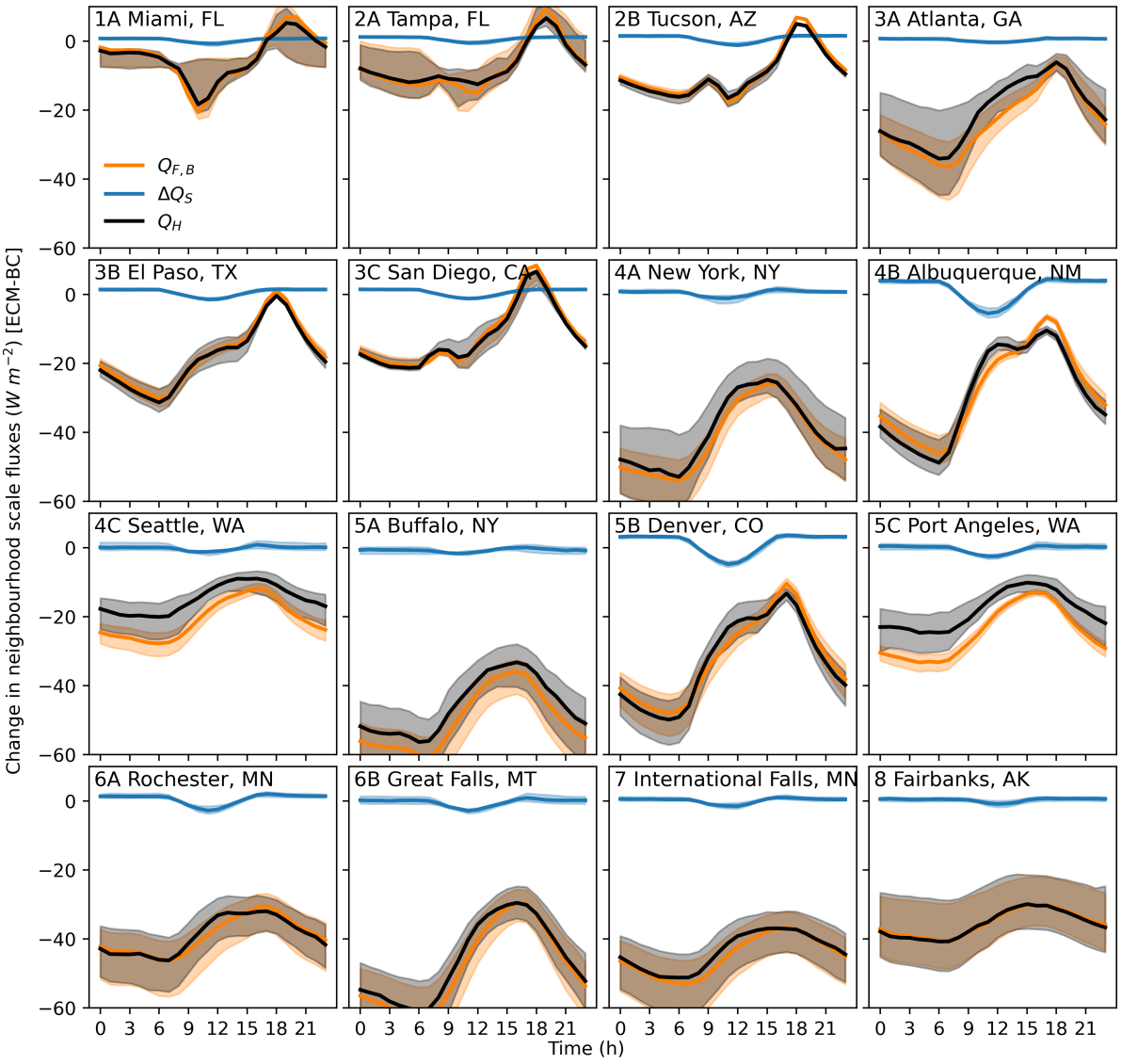

Fig. S2: Change in neighbourhood scale (with building plan area fraction of λ_p=0.3), wintertime (December, January, and February: DJF) anthropogenic ($Q_{F,B}$), storage (ΔQ_S) and turbulent sensible heat fluxes (Q_H) from retrofitting buildings ($n_{rertrofit}$=95%) in 16 USA cities showing median (line) and interquartile range (IQR, shading). Note change in Q_H results from the combined effect of changes in $Q_{F,B}$ and ΔQ_S.

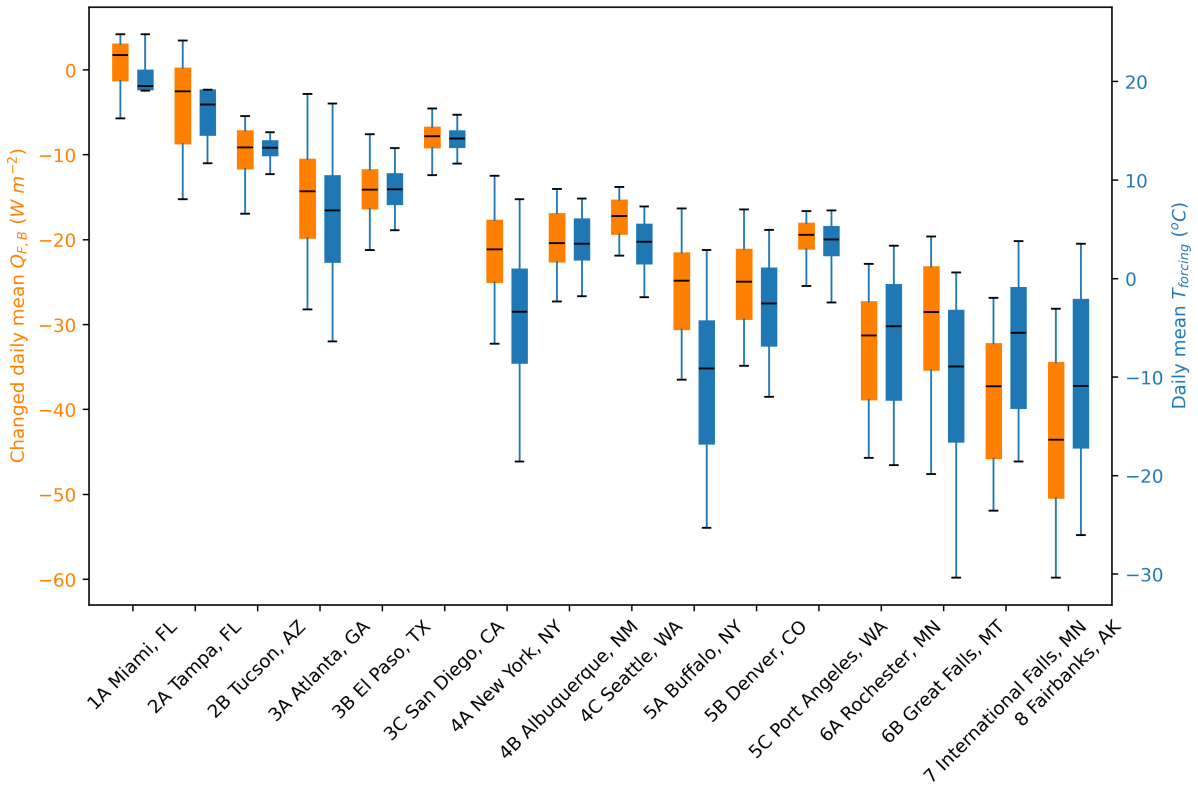

Fig.S3: Variability (median line), IQR (box) and 5th–95th percentiles (whiskers) in changes [after retrofit differ to before retrofit] of the DJF daily mean neighbourhood scale (λ_p=0.3, $n_{rertrofit}$=95%) anthropogenic heat flux ($Q_{F,B,}$ orange) and forcing height (33.5 m from ERA5[28]) air temperature ($T_{forcing}$, blue).

SI 5. Bias of vertical wind profiles from SUEWS to EnergyPlus

SUEWS provides high-resolution wind speed profiles for each neighbourhood scenarios defined in (Fig. S4) but are neither directly imported nor directly compatible with EnergyPlus' use of a power-law with one set of parameters and 10-m wind speed data[18]. Hence, the vertical profiles of wind speed differ substantially (Fig. S4).

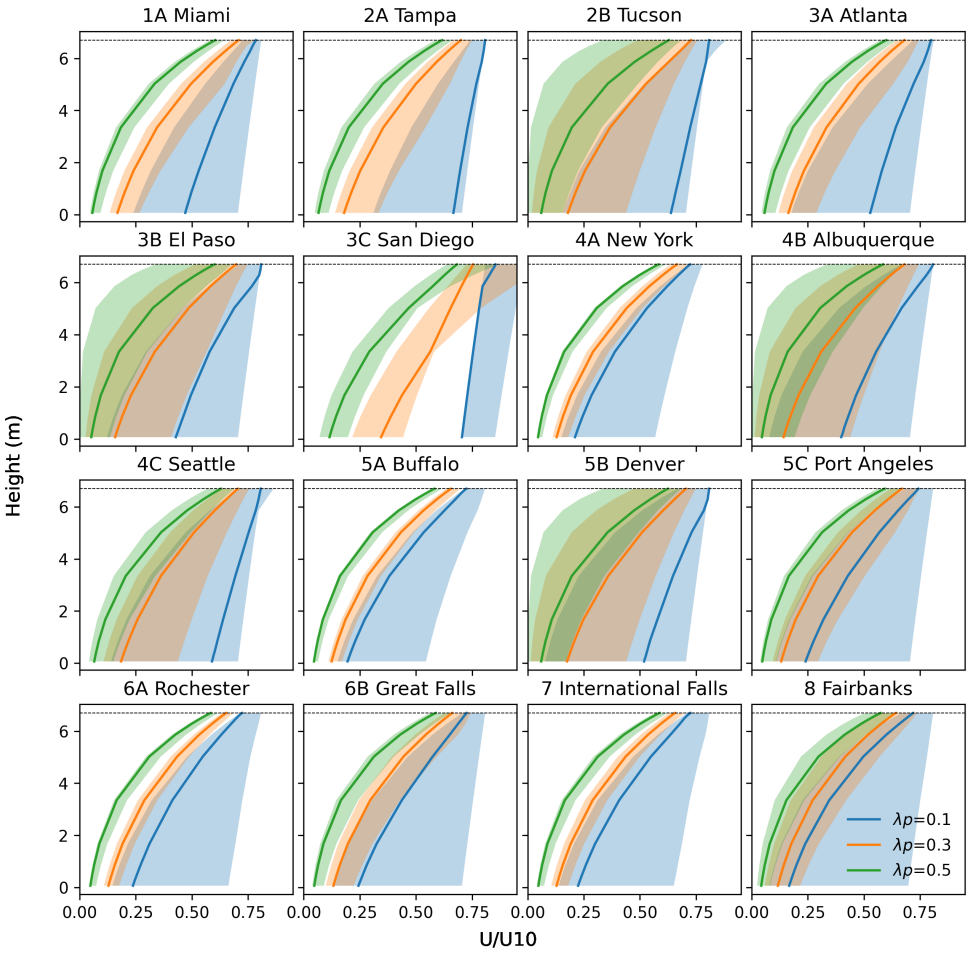

Fig. S4: Canopy layer vertical wind speed profiles (normalised by 10-m wind speed) with height (z) across 16 US cities showing median (line) and interquartile range (IQR, shading). Mean building height is 6.7m.

In EnergyPlus, wind speed (U_z) at height above ground z is estimated using[29]:

$$U_z = U_{met}\left[\frac{\delta_{met}}{z_{met}}\right]^{\alpha_{met}}\left[\frac{z}{\delta}\right]^{\alpha} \quad \text{(S9)}$$

using a site exponent (α), δ wind speed profile boundary layer thickness at the site; and meteorological data (*met*, default height z_{met} = 10 m) with a corresponding wind speed profile exponent (default α_{met} = 0.14) and boundary layer thickness (default δ_{met} 270m). However, even using fitted values of δ and α (Tang et al. 2021), the vertical profile shape is biased (Fig. S5). To address this issue, we modify the EnergyPlus source code (Eq. S9) to a form that better matches the SUEWS profiles:

$$U_z = U_{met}\left(\frac{z}{z_{met}}^{\alpha} + \beta\right) \quad \text{(S10)}$$

Using this form allows the wind speed bias at different heights to be improved, cf. using the default (Fig. S5), but bias remains because the profile coefficients (e.g. α, β) are fixed per simulation year. This static approach does not capture variability in atmospheric stability or weather conditions affecting wind profile shape.

Future work should make the coupling dynamic to provide time-varying wind profiles directly from SUEWS to EnergyPlus. This would eliminate the need to parameterise wind profiles and substantially improve the representation of wind-driven processes, particularly infiltration and convective heat transfer, in building energy simulations.

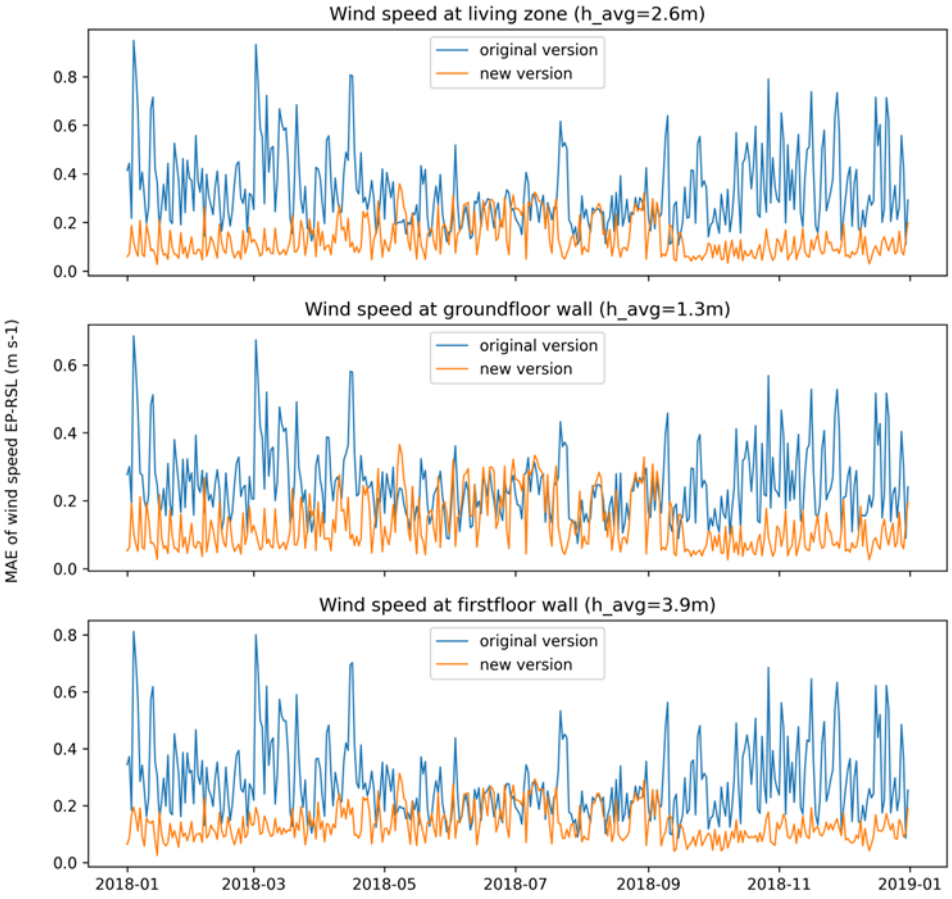

Fig. S5: Wind speed bias (EnergyPlus - SUEWS) for New York (λp=0.3, BC) when using Eq.S9 (blue) and Eq. S10 (orange).

References

1. Liu, Y., Luo, Z. & Grimmond, S. Revising the definition of anthropogenic heat flux from buildings: role of human activities and building storage heat flux. *Atmos. Chem. Phys.* **22**, 4721–4735 (2022).

2. El Fil, B. & Garimella, S. Waste heat recovery in commercial gas-fired tumble dryers. *Energy* **218**, 119407 (2021).

3. Sailor, D. J. & Vasireddy, C. Correcting aggregate energy consumption data to account for variability in local weather. *Environ. Model. Softw.* **21**, 733–738 (2006).

4. Ao, X. *et al.* Evaluation of the Surface Urban Energy and Water Balance Scheme (SUEWS) at a dense urban site in Shanghai: Sensitivity to anthropogenic heat and irrigation. *J. Hydrometeorol.* **19**, 1983–2005 (2018).

5. Kotthaus, S. & Grimmond, C. S. B. Atmospheric boundary-layer characteristics from ceilometer measurements. Part 2: Application to London's urban boundary layer. *Q. J. R. Meteorol. Soc.* **144**, 1511–1524 (2018).

6. Glazer, R. H. *et al.* Hectometric-scale modelling of the urban mixed layer evaluated with a dense LiDAR-ceilometer network. *EGUsphere* 1–26 (2025).

7. Kotthaus, S. & Grimmond, C. S. B. Atmospheric boundary-layer characteristics from ceilometer measurements. Part 1: A new method to track mixed layer height and classify clouds. *Q. J. R. Meteorol. Soc.* **144**, 1525–1538 (2018).

8. Liu, Y., Luo, Z. & Grimmond, S. Impact of building envelope design parameters on diurnal building anthropogenic heat emission. *Build. Environ.* **234**, 110134 (2023).

9. Wilson, E. J., Christensen, C. B., Horowitz, S. G., Robertson, J. J. & Maguire, J. B. *Energy Efficiency Potential in the US Single-Family Housing Stock*. (2017).

10. Reyna, J. *et al. US Building Stock Characterization Study: A National Typology for Decarbonizing Us Buildings*. (2022).

11. Grimmond, C. S. B., Cleugh, H. A. & Oke, T. R. An objective urban heat storage model and its comparison with other schemes. *Atmos. Environ. Part B, Urban Atmos.* **25**, 311–326 (1991).

12. Arnfield, A. & Grimmond, C. An urban canyon energy budget model and its application to urban storage. *Energy Build.* **27**, 61–68 (1998).

13. Meyn, S. K. & Oke, T. R. Heat fluxes through roofs and their relevance to estimates of urban heat storage. *Energy Build.* **41**, 745–752 (2009).

14. Anandakumar, K. A study on the partition of net radiation into heat fluxes on a dry asphalt surface. *Atmos. Environ.* **33**, 3911–3918 (1999).

15. Ward, H. C., Kotthaus, S., Järvi, L. & Grimmond, C. S. B. Surface Urban Energy and Water Balance Scheme (SUEWS): Development and evaluation at two UK sites. *Urban Clim.* **18**, 1–32 (2016).

16. Järvi, L., Grimmond, C. S. B. & Christen, A. The Surface Urban Energy and Water Balance Scheme (SUEWS): Evaluation in Los Angeles and Vancouver. *J. Hydrol.* **411**, 219–237 (2011).

17. Theeuwes, N. E., Ronda, R. J., Harman, I. N., Christen, A. & Grimmond, C. S. B. Parametrizing Horizontally-Averaged Wind and Temperature Profiles in the Urban Roughness Sublayer. *Boundary-Layer Meteorol.* **173**, 321–348 (2019).

18. Tang, Y. *et al.* Urban meteorological forcing data for building energy simulations. *Build. Environ.* **204**, 108088 (2021).

19. Lavor, V., Luo, Z. & Grimmond, S. Mapping Urban Airborne Infection Risk in Greater London, UK: Influence of urban form, weather, and population density (2025), (to be published).

20. Hang, J. *et al.* Evaluation of surface urban energy and water balance scheme (SUEWS) using

scaled 2D model experiments under various seasons and sky conditions. *Urban Clim.* **54**, 101851 (2024).

21. Obe, O. B., Morakinyo, T. E. & Mills, G. A study of the impact of landscape heterogeneity on surface energy fluxes in a tropical climate using SUEWS. *Urban Clim.* **53**, 101788 (2024).

22. Xie, X., Luo, Z., Grimmond, S. & Sun, T. Impact of building density on natural ventilation potential and cooling energy saving across Chinese climate zones. *Build. Environ.* **244**, 110621 (2023).

23. Ward, H. C. & Grimmond, C. S. B. Assessing the impact of changes in surface cover, human behaviour and climate on energy partitioning across Greater London. *Landsc. Urban Plan.* **165**, 142–161 (2017).

24. Xie, X. *et al.* Could residential air-source heat pumps exacerbate outdoor summer overheating and winter overcooling in UK 2050s climate scenarios? *Sustain. Cities Soc.* **115**, 105811 (2024).

25. Oke, T. R. The urban energy balance. *Prog. Phys. Geogr. Earth Environ.* **12**, 471–508 (1988).

26. Loridan, T. & Grimmond, C. S. B. Characterization of energy flux partitioning in urban environments: Links with surface seasonal properties. *J. Appl. Meteorol. Climatol.* **51**, 219–241 (2012).

27. Harman, I. N. & Finnigan, J. J. A simple unified theory for flow in the canopy and roughness sublayer. *Boundary-Layer Meteorol.* **123**, 339–363 (2007).

28. Hersbach, H. *et al.* The ERA5 global reanalysis. *Q. J. R. Meteorol. Soc.* **146**, 1999–2049 (2020).

29. U.S. Department of Energy. *EnergyPlus™ Version 9.5.0 Documentation Engineering Reference*. (2021).